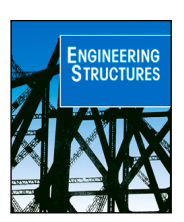
ELSEVIER

Contents lists available at ScienceDirect

Engineering Structures

journal homepage: www.elsevier.com/locate/engstruct





New fatigue load models for assessing railway bridges in Europe

Stefan Verdenius a, Sjoerd Hengeveld a,b, Johan Maljaars a,b,*

- a TNO, Molengraaffsingel 8, Delft, 2629 JD, The Netherlands
- ^b Eindhoven University of Technology, PO Bos 513, Eindhoven, 5600 MB, The Netherlands

ARTICLE INFO

Keywords:
Fatigue load model
Axle load measurements
Railway bridges
Equivalent axle load
Reliability analysis

ABSTRACT

Train axle load measurements performed between 2012 and 2019 at 87 locations in the Dutch railway network are used to evaluate fatigue of railway bridges. The theoretical fatigue damage using realistic influence lines is determined for the measured loads and for the load model from Eurocode EN 1991-2 Annex D. It appears that this load model is (very) conservative for most cases, but unconservative for a few cases. Large differences in fatigue relevant loads are observed between different tracks. Two alternative load models that more closely represent the measured railway traffic in terms of trains and fatigue damage are presented, together with a third model based on historical train types. These models use track-specific traffic characteristics. Uncertainties are quantified and safety factors are established from a reliability analysis.

1. Introduction

Fatigue is an important failure mechanism for (metal) railway bridges [1–3]. To determine the fatigue damage, knowledge of the loads exerted by the vehicles crossing the structure is of uttermost importance [4]. Load models closely representing the effects of real vehicle loads are required for the assessment, i.e. remaining lifetime estimation, of existing structures [5,6]. This paper focuses on load models for assessments, although the methodology can also be applied to designs of new bridges.

Load effect measurements e.g. using strain gauges are considered the most accurate source of data on the load side for the fatigue assessment of individual bridges [7,8]. Case studies therefore often use such data, see amongst others [9–17]. However, it is usually efficient to first carry out a desk study, followed by field measurements only if the desk study reveals a potential fatigue issue [18,19]. Load models from standards can be used in desk studies.

In Europe, the standard EN 1991-2 [20] is used for the loads in the fatigue design of a bridge. It contains two fatigue load models; a relatively simple factored Load Model '71 (or, alternatively, a factored Load Model 2000 [21]) called lambda model, and a more laborious but more realistic model from Annex D of the standard consisting of 12 standard trains with associated occurrences depending on the traffic composition of the track. Although these models are developed for the design of new bridges, because of a lack of alternatives the Annex D model [22,23] and even the lambda model [24] are used for the assessment of existing bridges. Some countries have national load models, such as the model in the Italian Instruction 44/F [25] also

described in [26], and the British Standard BS 5400 [27], used in [28]. Load models from standards are sometimes combined with information from asset owners [29–31]. Alternatively, load models from earlier studies are used to verify a bridge for fatigue [32,33].

Obviously, the estimate or prediction of fatigue relevant loads contains inherent uncertainties. These uncertainties can be reduced by relatively simple measurements, such as counting of the number of passing axles, but also by using load measurements through Weigh-In-Motion (WIM) systems, preferably directly at the location of interest [34–39]. However, to arrive at a representative load model these measurements should be combined with historical data on rail vehicle loads [11,40,41] because train numbers, train types and axle loads have changed over time. Imam et al. suggest to divide the period of assessment in three [42] or four [30] distinct periods, each associated with particular characteristics in rail traffic.

Different studies have been devoted to the development of fatigue load models for assessing railway bridges in the United States [43–45] and Europe [40,41,46–48]. Some of these models are based on general data of train types and numbers, others are based on WIM measurements. The studies listed for Europe that are based on WIM measurements used data from one or a few measurement locations. The load model proposed in [46] is shown to be overly conservative by a verification with two bridges at other locations in [49]. This demonstrates that the fatigue relevant loads are track-specific. In the author's experience, large differences in daily traffic are present between different tracks. A generic load model applicable to each track as in EN 1991-2 [20] may be sufficient for the design of new structures. A

^{*} Corresponding author at: Eindhoven University of Technology, PO Bos 513, Eindhoven, 5600 MB, The Netherlands. E-mail address: johan.maljaars@tno.nl (J. Maljaars).

differentiation in load model based on track characteristics, however, may be beneficial for the assessment of existing structures. No work has been found in which rail fatigue load models are verified against comprehensive axle load measurements collected over a long period and at various locations with specified traffic characteristics per track.

Fatigue damage calculations are performed in the current study for various influence lines, using a standard S–N curve for welded and riveted connections and axle load measurements performed at 87 locations in The Netherlands between the years 2012 and 2019. The joint DataBase (DB) comprises of $1.2 \cdot 10^9$ passing axles and a summed axle load of $8.6 \cdot 10^{12}$ kg (8600 megatonnes). The DB load effects are compared to those of the load model from EN 1991-2 Annex D [20] in terms of fatigue damage. Two new load models for fatigue assessment of railway bridges are developed, which give a better representation of the DB load effects. A third load model is added representing the damage exerted by historical train types.

2. Description and evaluation of measurements

Dynamic axle load measurements are performed in a system using two times six optical sensors, each set of six installed on one of the two rails in the spans between seven subsequent sleepers. The sensors register the peak deflection of the rail due to passing trains, from which axle loads, axle distances and train speeds are derived [50]. The static axle loads are estimated as the average value recorded by the six sensors, thereby suppressing dynamic amplifications e.g. caused by non-round wheels. The system also registers the train type. The system has a guaranteed measurement accuracy, which will be discussed later in this paper.

Several of these systems are installed in the rail network in The Netherlands. The blue dots in Fig. 1 represent the spatial locations of the measurement systems (each blue dot represents at least two measurement systems for the two traffic directions). The lines in Fig. 1 represent tracks. The tracks have an allowed distributed load varying between 64 and 90 kN/m. The red lines are tracks exclusively used for cargo transport. The longest of these cargo tracks, between the North Sea and the German border, contains several measurement systems. This track is characterized by long cargo trains and a high annual summed mass of up to $m_{yr} = 32 \cdot 10^9$ kg for the direction heading east. This is the only track with a permissible maximum axle load of $F_{max} = 250$ kN; all other tracks have $F_{max} = 225$ kN (or $F_{max} = 200$ kN for a few tracks). The blue lines represent regional tracks, mostly exploited by a single (regional) operator. These are characterized by a low frequency of passing trains, dominated by one specific type of train. These tracks have an annual summed mass per direction as low as $m_{vr} = 2 \cdot 10^9$ kg. The green line is a high-speed track, which is not considered in this study. All other lines are tracks for 'standard' traffic consisting of a mix of cargo and passenger trains.

Data quality checks have been performed on the data. No abnormalities such as exceptionally small or large axle distances have been encountered. However, trains with a speed lower than 30 km/h and trains with speed differences of more than 40% between the first and the last axle are removed from the database as the systems may not accurately estimate the characteristics of such trains. The number of trains dismissed because of these criteria is less than 0.5%.

Fifty different non-cargo (i.e. passenger and maintenance) train types are registered in the joint DB. Using expert judgement, similar train types are combined, thereby reducing the number of passenger train types to 21. Maintenance trains are ignored because of the negligible number of occurrences. More than forty different types of cargo train are registered which could not easily be grouped because of their different characteristics. Some trains are registered as 'unknown', which are expected to be cargo trains based on their characteristics (e.g. the number of axles). Table 1 gives an overview of the remaining 23 train types. Special attention should be payed to the VIRM, which is a double deck train with heavy axles and large boogie distances. It may therefore cause higher fatigue damage as compared to other passenger train types. Similar double deck train types are currently used in many European countries.

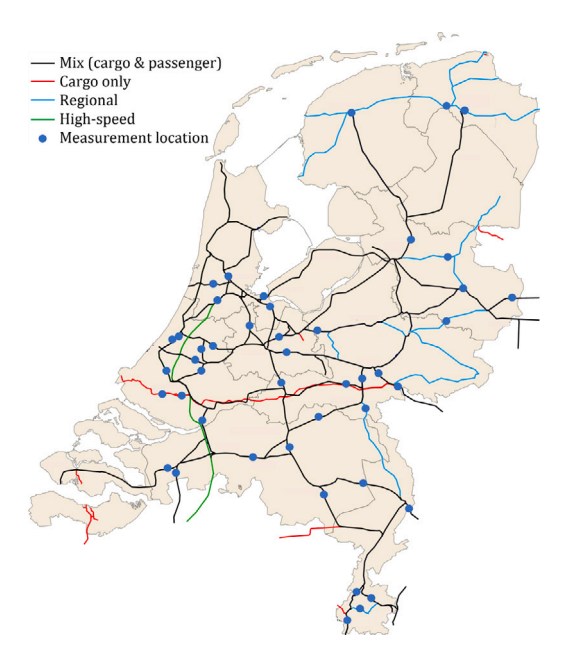


Fig. 1. Overview of all measurement systems on a ground plan of The Netherlands.

Table 1 Train types registered by the measurement system (characteristics available in [51]). VIRM DM90ICR Thalys DDAR ICK Mat64 GTW 2/8 GTW 2/6 SLT Lint Belgian SGM DDZ

Protos

cargo

'unknown

3. Evaluation of the Eurocode model

Eurostar

The fatigue load model in Annex D of EN 1991-2 [20] – hereafter abbreviated as EC – consists of 12 train types, each defined as a set of axles with certain axle load and certain distance between the axles. Three traffic compositions are defined, being:

- Standard traffic mix for tracks with $F_{max} = 225$ kN.
- Heavy traffic mix for tracks with $F_{max} = 250$ kN.

Fyra

• Light traffic mix for dedicated tracks, again with $F_{max} = 225$ kN. This composition is mainly used for light rail and subway tracks and it is not used in this paper.

The number of trains per type is a function of the composition. The annual summed mass of the axles is $m_{yr}=25\cdot 10^9$ kg for all three compositions. The axle loads are multiplied with a dynamic amplification factor ϕ depending on the influence length L and the (predefined) train speed v:

$$\phi = 1 + \frac{0.5K}{1 - K + K^4} + 0.14 \exp(-0.01(L/m)^2)$$
 (1)

$$K = \begin{cases} \frac{v}{160 \text{ m/s}} & \text{if } L \le 20 \text{ m} \\ \frac{0.0212}{(L/\text{m})^{0.408}} \frac{v}{\text{m/s}} & \text{otherwise} \end{cases}$$
 (2)

The theoretical fatigue damage is determined for the EC fatigue load model due to 100 years of operation. An algorithm is developed for this purpose, which is validated against strain measurements on a bridge in [52]. It consists of the following steps:

- The array of axles (including the dynamic amplification factor) that compose a train is pulled over an influence line.
- The resulting stress history is recorded.
- Rainflow counting is applied to convert the stress history to a stress range histogram. These three steps are repeated for each train in the model.

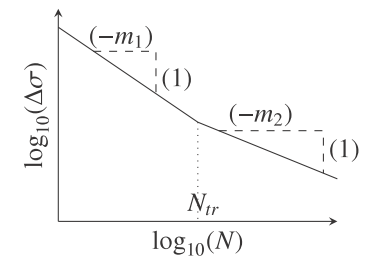


Fig. 2. S-N curve parameters m_1 , m_2 and N_{tr} .

Table 2 S–N curve parameters.

Connection	m_1	m_2	N_{tr}
Welded	-3	-5	$5 \cdot 10^{6}$
Riveted	-5	-7	$5 \cdot 10^6$

- The fatigue damage per cycle j, $1/N_j$, is determined using the bi-linear Basquin-type S–N curve of Eq. (3).
- The accumulated fatigue damage *D* is determined using Palmgren–Miner's linear damage accumulation rule [53,54], Eq. (4).

$$N_{j} = \begin{cases} C_{1} \Delta \sigma_{j}^{m_{1}} & \text{if } C_{1} \Delta \sigma_{j}^{m_{1}} \leq N_{tr} \\ \frac{m_{2}}{C_{1}^{m_{1}}} \frac{m_{1} - m_{2}}{M_{1r}} \Delta \sigma_{j}^{m_{2}} & \text{otherwise} \end{cases}$$
(3)

$$D = \sum_{j} \frac{n}{N_{j}} \tag{4}$$

where N_i is the number of cycles to failure for cycle j with stress range $\Delta\sigma_i$ and *n* is the multiplication factor for the number of applied cycles, equal to n = 36525 for a life of 100 years because the EC load model is defined per day. Parameters N_{tr} , m_1 , m_2 and C_1 define the S-N curve, Fig. 2. The current study considers welded and riveted connections. For most weld connections in structural steel it is well established that $m_1 = -3$, $m_2 = -5$ and $N_{tr} = 5 \cdot 10^6$ or 10^7 . A larger variation in parameters is observed for riveted connections [55]. Slope parameter m_1 is determined as $m_1 = -3$ in [18], $m_1 = -4$ in [56], $(m_1 = -3$ for very high stress range levels and further) $m_1 = -5$ in [57], and $m_1 = -7$ in [58]. Equivalent to bolted connections [59] this large variation is caused by differences in hole forming method, friction coefficient and rivet clamping force. A lack of variable amplitude test data causes high uncertainty in m_2 . Some authors adopted Haibach's proposal m_2 = $2m_1 + 1$ [60], originally proposed for welded connections, whereas others extended the curve with $m_2 = m_1$. A slope parameter $m_2 = m_1 - 2$ is sometimes adopted. A value of $N_{tr} = 5 \cdot 10^6$ is estimated from limited test data in [61]. In evaluating the load models, the current study uses an average of the proposed S-N curve parameters, Table 2.

Based on results from a preliminary study, influence lines are considered at midspan of a single span and a three span beam in bending (Fig. 3) with spans L=5, 10, 15, 20, 30 or 50 m. This selection is based on an overview of typical railway bridges [62]. The stress range follows from the bending moment range divided by the elastic section modulus, W. Selecting a certain value for C_1 , the elastic section modulus W is calibrated such, that D=1 using the EC fatigue load model for standard traffic mix.

The theoretical fatigue damage is also calculated using the recorded trains in the DB for each of the 87 measurement locations, following the same procedure as described above with the exception that W is not altered, i.e. taken the same as for the EC standard traffic mix load model. The dynamic amplification factor according to Eqs. (1)–(2) is applied using the recorded speed per train. The multiplication factor for the number of applied cycles n is equal to 36525/2706 = 13.5 to simulate 100 years of operation, where 2706 is the number of days

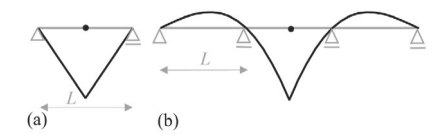


Fig. 3. Considered influence lines: (a) single span beam; (b) three span beam.

of measurement and 36525 is the number of days in 100 years of operation.

Fig. 4(a) provides the theoretical damages resulting from the simulations for a single span beam. The orange dashed curve represents the damage using the EC standard traffic mix (1 by definition) and the blue solid curve represents that of the EC heavy traffic mix. Each dot represents the damage of a measurement location from the DB, using the trains recorded at that location. Considering the permissible maximum axle loads, the blue dots (cargo only track) should be compared to the EC heavy traffic mix and the orange dots (all other tracks) should be compared to the EC standard traffic mix. Fig. 4(b) gives a probability density plot of the same data together with those of the three span beam, using the ratio of the damage according to the DB and the damage according to the EC models (standard or heavy traffic mix, where applicable), D_{DB}/D_{EC} , for all locations and all influence lines. The mean value M of this damage ratio is M=0.16 and the coefficient of variation V = 1.3 for a welded connection. These values are M = 0.09 and V = 1.9 for a riveted connection using the parameters of Table 2 (Note that the results of a riveted connection using the S-N curve in [18,63], with slopes $m_1 = -3$ and $m_2 = -5$, are equal to that of the welded connection).

Assuming the dots in Fig. 4(a) represent the damage caused by the actual traffic, it is evident that the EC model leads to a safe yet for most locations a very conservative approximation of the fatigue damage at all examined influence lines. In case of locations with limited and predominantly light traffic, the EC model overestimates the damage with a factor up to 100. On the other hand, the damage ratio D_{DB}/D_{EC} approaches 1 or, for a three-span beam, even exceeds 1 at some locations. The level of conservatism appears to depend on the influence length, thereby indicating that the train configurations in the load model are not representative for the actual traffic. Fig. 4 demonstrates a potential for improvement of the load model. As a first suggestion, the number of trains in the load model can be scaled using the annual summed mass per measurement location, i.e. multiplied with the ratio between the annual summed mass of the EC model and that of the DB. This gives some improvement of the load model performance, with the damage ratio D_{DB}/D_{EC} giving M=0.32 and V = 1.0 for a welded connection and M = 0.17 and V = 1.6 for a riveted connection. It appears that the damage has some, but not a very high, correlation with the annual summed mass per location, see Fig. 5(a). As an example, the correlation coefficient is 0.66 for a welded connection in a single span beam with L = 5 m. Fig. 5(b) and (c) show that a certain correlation is also present between D_{DB} and the number of axles per year n_{ax} and the average axle load F_{av} . This demonstrates that the model cannot be simply improved by modifying the axle loads or the number of trains. A differentiation with respect to track characteristics is required to improve the load model's performance.

4. Proposed load models

Three load models are developed by the authors based on the presented measurements. Load Model I is intended for use of any track for which detailed measurement information on axles loads and number of axles is available. Load Model II makes use of an (estimate of the) annual summed mass and some characteristics of the track. This model can be used for tracks or for periods without dedicated axle load measurements. These models should not be used to determine fatigue

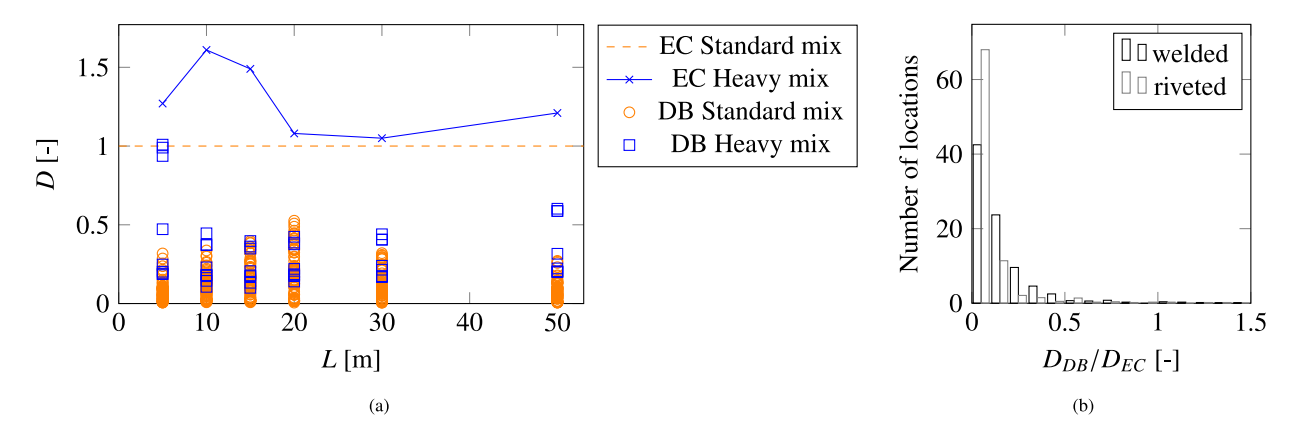


Fig. 4. Fatigue damage calculated using the EN 1991-2 Annex D (EC) load models compared to the damage calculated with the axle load measurements (DB): (a) For welded connection in a single span beam with different spans L; (b) Occurrences of the ratio D_{DB}/D_{EC} .

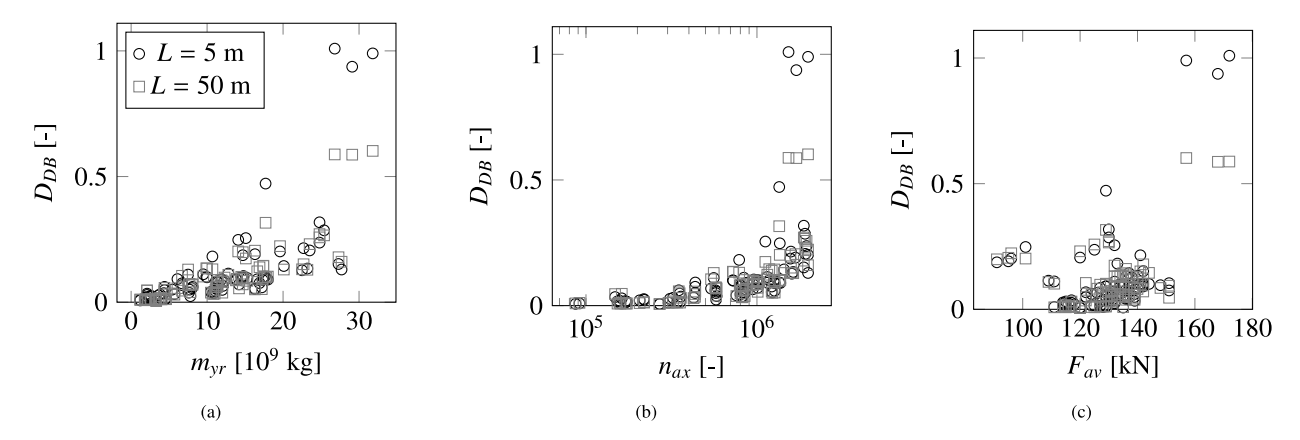


Fig. 5. Damage computed with the measured axle loads for a welded connection in a single span beam: (a) versus the annual summed mass; (b) versus the number of axles; (c) versus average axle load.

damage accumulated before 1970 due to a difference in train types before and after that date [40]. Load Model III is developed for the period before 1970 and it is based on limited available data and expert judgement. The damage caused by the load models accumulated during the associated periods can be summed. The load models contain realistic train types and compositions and they result in realistic, slightly conservative damage assessments. They are developed for ease of use although the assessment of different periods implies that the models are more laborious than the model of EN 1991-2 Annex D [20].

4.1. Fatigue Load Model I: Equivalent axle load

Load Model I originates from the basic principle that fatigue damage differs per location, not only due to a difference in annual summed mass, but also due to a difference in number of axles and axle loads. The concept of equivalent axle load F_{eq} per measurement location is therefore introduced:

$$F_{eq} = \left(\frac{\sum_{i=1}^{n_{ax}} \left[(F_{ax,i} \psi)^{n_2} \right]}{n_{ax}} \right)^{\frac{1}{n_2}}$$
 (5)

where $F_{ax,i}$ represents the axle load of axle i at a certain measurement location and n_{ax} is the annual number of axles passing that location. S–N curve slope parameter m_2 is used to reflect the larger contribution to the damage accumulated with the second stage of the S–N curve. Factor ψ accounts for the larger variability in loads between subsequent (full and empty) wagons of the same train in case of cargo traffic compared to passenger traffic (sequence effect). This larger variability causes larger stress cycles and hence larger fatigue damage [44] for the same (average) axle load. Factor ψ is taken as 1 by definition for

passenger trains and it should be taken as 1.14 for cargo trains, the value derived in the background report of this study [64].

The addition of the factor ψ appears crucial for a good indication of damage contribution. Evaluating the fatigue damage at all 87 measurement locations, Fig. 6, a clear correlation appears between the combination of equivalent axle load and number of axles on the one hand (axes) and the fatigue damage on the other hand (colors). The figure shows that a high equivalent axle load in combination with little traffic (e.g. location S233) leads to a similar fatigue damage as a high traffic frequency with a low equivalent axle load (e.g. location S204), almost irrespective of the influence length. The equidistant diagonal lines in Fig. 6 distinguish locations with similar fatigue damage. Based on this concept, Load Model I consists of six categories A to F separated by the diagonal lines expressed through:

$$B = n_{ax} \left(\frac{F_{eq}}{kN}\right)^{-m_2} \tag{6}$$

with values of $\log_{10}(B)$ according to Table 3. The same systematic of selecting a category can be applied to tracks elsewhere in Europe for which the number of axles and the axle loads are measured by plotting these two characteristics in the same graph. Fig. 6 shows the results for a welded detail, using $m_2 = -5$. The equivalent axle loads, damages and category separations are different for $m_2 = -7$. However, the allocation of measurement locations to a category changes only marginally. It is therefore not necessary to use separate categorization for welded and riveted connections.

Each category is represented by a characteristic traffic mix in Load Model I. A compromise is sought between keeping the number of train types in the new load model limited – for ease of use – and obtaining a reasonable representation of the actual (recorded) traffic. The 21

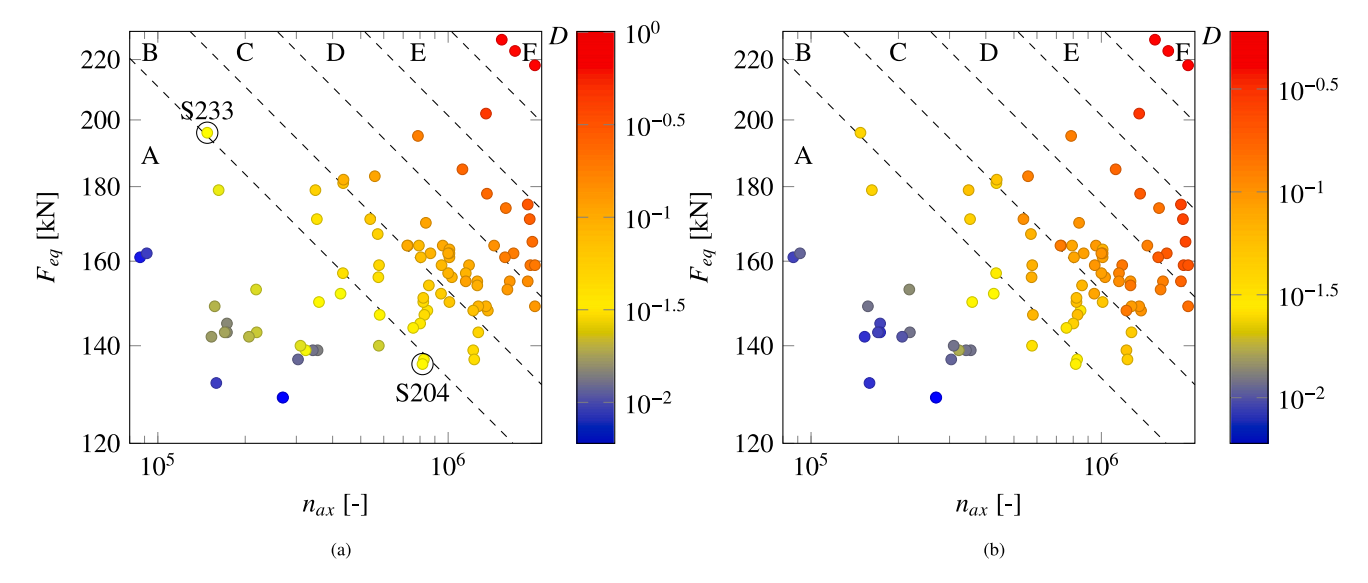


Fig. 6. Fatigue damage for an S-N curve with $m_2 = -5$ plotted as a function of the equivalent axle load and annual number of axles per measurement location: (a) For a single span beam with L = 5 m; (b) For a single span beam with L = 50 m.

Table 3 Values of $\log_{10}(B)$ in Eq. (6) – Distinction of categories.

Connection	Cat. A–B	Cat. B–C	Cat. C–D	Cat. D–E	Cat E–F
Welded $(m_2 = -5)$	16.62	16.92	17.22	17.52	17.82
Riveted $(m_2 = -7)$	20.92	21.32	21.72	22.12	22.52

passenger trains from Table 1 are therefore reduced to seven train types, some of them equal to the train types in the EC model, whereas others are new and defined by the authors. Additionally, five cargo trains are defined that resemble the cargo traffic, see the Appendix. The selection is based on the typical number of axles, axle loads and axle distances per train type, determined by plotting histograms of these characteristics of each train type in the DB. As an example, the cargo trains in Load Model I contain more axles than the cargo trains in the EC load model, thereby showing more resemblance with the cargo trains found in the DB (on average 92 axles per train with a standard deviation of 59 axles). Train speeds are based on the recorded speeds of comparable trains in the DB [65] or the speeds in the EC model. The number of trains per type in Load Model I, n_t , is calibrated such that the damage that each train type t resembles equals the damage caused by its corresponding train type in the DB, using:

$$n_t = \sum \frac{n_k D_k}{D_t} \tag{7}$$

where D_t represents the damage of a train type $t \in (1..12)$ in the Appendix and D_k represents the damage of those train types k (with numbers n_k) of Table 1 that should be resembled by train type t. The number of trains n_t is subsequently scaled in such a way that the load model results in a fatigue damage equal to that of the measurement location with the highest damage in the category. Finally, the numbers are rounded to an integer number of trains per type per day. Table 4 gives the resulting load model. The model is deemed applicable to other countries in Europe because permissible axle loads and passenger train types are similar in most European countries and the cargo trains in The Netherlands are predominantly cross-border, i.e. international. Traffic composition and number of trains per day differ between countries (and tracks) but these aspects are explicitly accounted for in the model. However, the applicability of the model to other countries has not yet been checked due to lacking data.

Fig. 7 gives an indication of the performance of this new load model for a welded connection, where each subfigure shows the fatigue damage of a category in a similar way as in Fig. 4. The figure displays

Table 4
Load Model I, with daily train numbers per type and per category.

Category	A	В	С	D	E	F
Type 2	1	2	14	12	_	-
Type 4	-	-	1	1	-	-
Type 9 - 0.9	7	3	3	-	-	_
Type 9 - 1.0	28	47	56	56	-	_
GTW	61	-	5	3	-	_
DDAR/DDZ	5	7	12	11	-	_
VIRM	14	40	70	46	-	-
Cargo full - 2 ax	-	-	-	1	1	2
Cargo full - 4 ax	-	-	1	1	4	10
Cargo full - 6 ax	-	-	-	-	2	5
Cargo mixed	-	1	1	6	5	8
Cargo empty	3	-	-	6	7	3

the fatigue damage resulting after 100 years for the EC standard traffic mix ($D_{EC}=1$ by definition), the new Load Model I D_{LMI} and the DB at each location D_{DB} . Fig. 8 gives the same data for a riveted connection.

The figures show that Load Model I is less conservative compared to the EC model and that it better resembles the trend in damage at different influence lengths. Similar results are obtained for a three span beam (results not displayed). The ratio D_{DB}/D_{LMI} for all measurement locations and influence lines considered has a mean of M=0.68 and a coefficient of variation of V=0.54 in case of a welded connection. These values are M=0.41 and V=0.67 for a riveted connection. Hence, additional to being less conservative, Load Model I gives lower scatter compared to the EC model. The performance of the new load model is even better if considering the 20% heaviest loaded locations – where fatigue may be more relevant – M=0.64 and V=0.33 in case of a welded connection.

4.2. Load Model II: annual summed mass

Load Model I gives a good resemblance of the damage caused by the DB trains, but it requires axle load measurement data. Load Model II is developed for the case that such data are not available. It is based on the requirement that the categories must be distinguishable through general characteristics of the track. Four categories are distinguished:

 Cat A+ Regional tracks characterized by a low frequency of passing trains, mostly exploited by a single (regional) operator and dominated by one specific type of train.

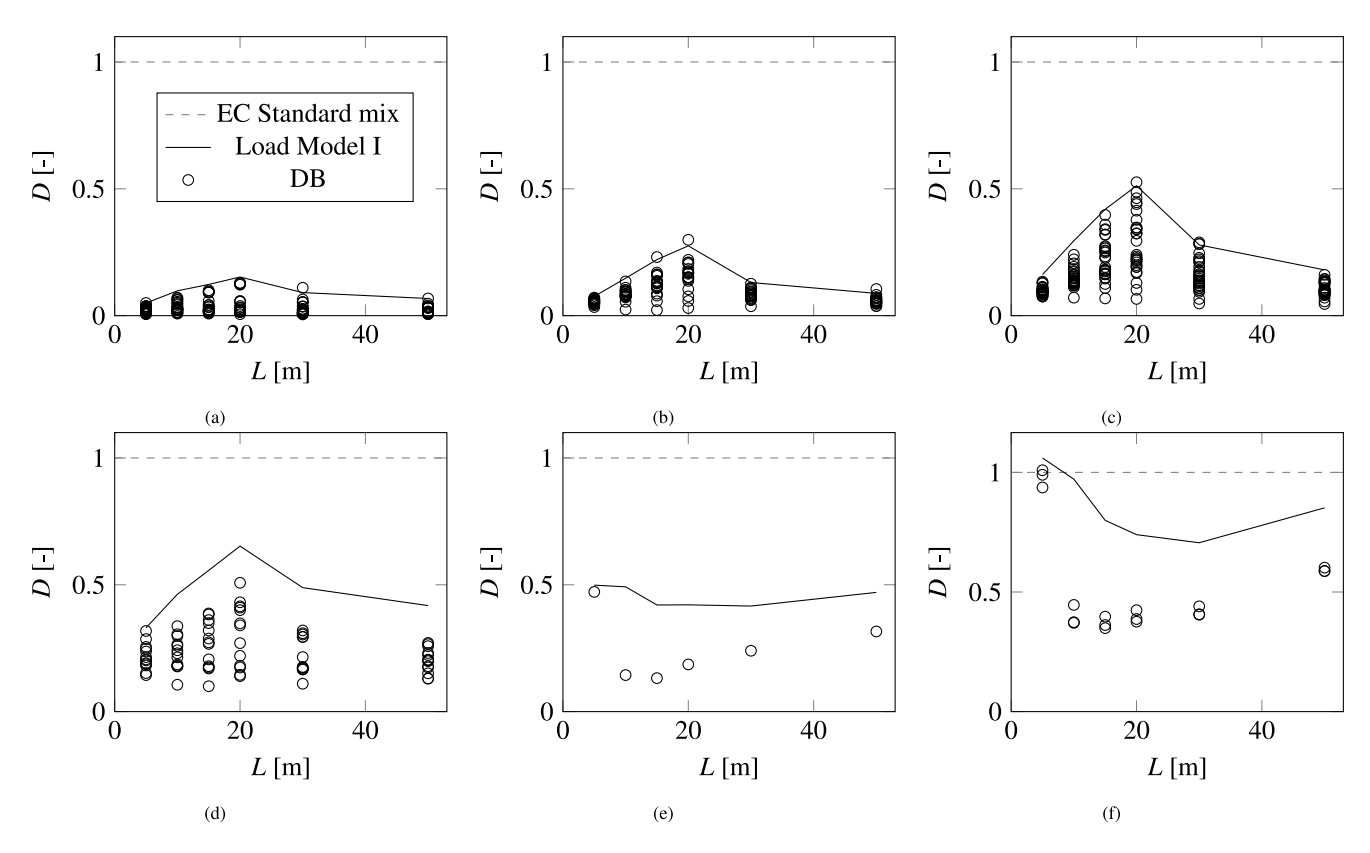


Fig. 7. Fatigue damage of a welded connection in a single span beam using the EC standard traffic mix, Load Model I and the DB: (a) Category A; (b) Category B; (c) Category C; (d) Category D; (e) Category E; (f) Category F.

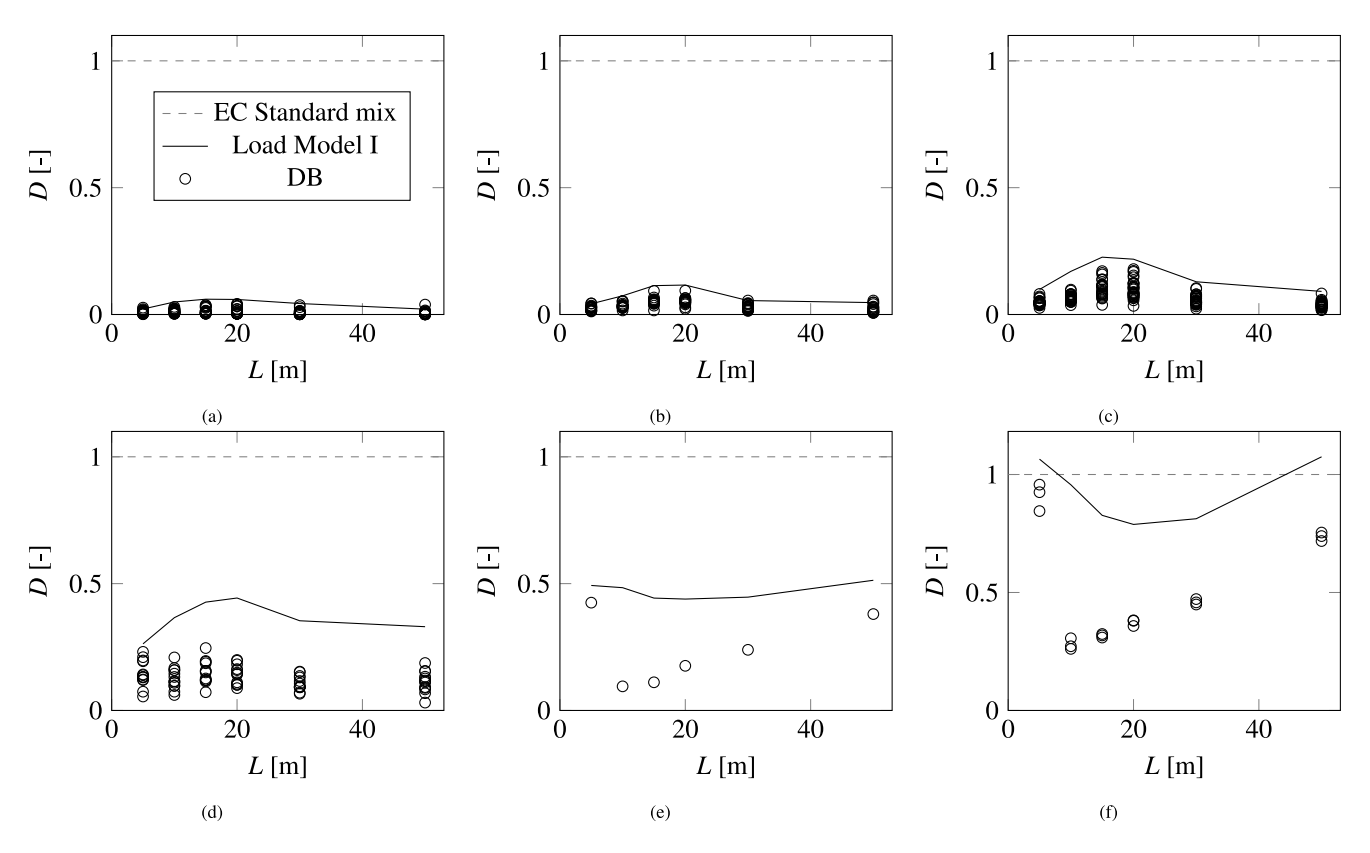


Fig. 8. Fatigue damage of a riveted connection in a single span beam using the EC standard traffic mix, Load Model I and the DB: (a) Category A; (b) Category B; (c) Category C; (d) Category D; (e) Category E; (f) Category F.

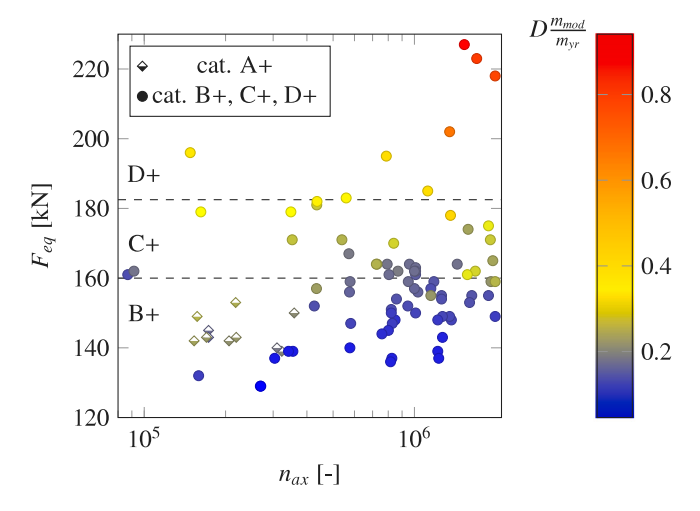


Fig. 9. Normalized fatigue damage for an S–N curve with $m_2 = -5$ and a single span beam with L = 5 m plotted as a function of equivalent axle load and annual number of axles per measurement location.

- Cat B+ Predominantly passenger traffic with little to no cargo trains
- Cat C+ Either a mix of passenger and cargo trains, usually longdistance, or main passenger tracks with a high frequency of double deck trains.
- Cat D+ Dedicated cargo track with heavy loads, $F_{ax,max}$ =250 kN.

The categorization is loosely based on the equivalent axle load. The differentiation between Cat. B+ and C+ is roughly at $F_{eq}=160$ kN and that between Cat. C+ and D+ is at $F_{eq}=185$ kN. Locations with similar traffic composition may have different train numbers and hence different damage values. To take this into account, the load model is scaled with the annual summed mass. For this purpose, Fig. 9 provides the same data as Fig. 6(a) but with the damage multiplied with the ratio m_{mod}/m_{yr} , where m_{yr} is the annual summed mass of the measured location and $m_{mod}=25\cdot10^9$ kg. The figure shows a reasonable correlation between F_{eq} and the damage normalized to the mass m_{mod} .

As for Load Model I, the four categories of Load Model II are represented by a characteristic traffic mix, for which the same approach is followed as described in Section 4.1. The number of trains per category is scaled to result in an annual summed mass of $m_{mod} = 25 \cdot 10^9$ kg. Table 5 gives the resulting traffic mix. In applying the model at a specific location with annual summed mass m_{yr} , the number of trains in the model $n_{t,mod}$ (or the damage) should be scaled according to:

$$n_t = n_{t,mod} \frac{m_{yr}}{m_{mod}} \tag{8}$$

Hence, application of Load Model II requires a selection of the category and an estimate of the annual summed mass.

The performance of Load Model II is evaluated in a similar way as that of Load Model I, but with the damages of the DB scaled to an annual summed mass of $25 \cdot 10^9$ kg for each location. Figs. 10 and 11 give the results for a welded connection and a riveted connection, respectively, in a single span beam. The ratio D_{DB}/D_{LMII} for all measurement locations and influence lines considered has M=0.68 and V=0.45, respectively, in case of a welded connection. These values are M=0.47 and V=0.65 for a riveted connection. Similar to Load Model I, Load Model II more accurately resembles the fatigue damage caused by the actual traffic compared to the EC model. Load Model II underestimates the damage for a limited number of locations and influence lines. This is accounted for through the partial factor in Section 5.

Table 5
Load Model II, with daily train numbers per type and per category.

Category	A+	B+	C+	D+
Type 2	-	5	28	_
Type 4	-	-	1	-
Type 9 - 0.9	-	35	-	-
Type 9 - 1.0	33	75	38	-
GTW	590	3	21	-
DDAR/DDZ	-	18	-	_
VIRM	-	61	77	-
Cargo full - 2 ax	-	-	1	3
Cargo full - 4 ax	-	-	1	5
Cargo full - 6 ax	-	1	1	6
Cargo mixed	2	2	1	12
Cargo empty	1	-	1	12
m _{mod} [10 ⁹ kg]	25.0	25.0	25.0	24.7

4.3. Load Model III: historic train types

Load Model III is to be used for the damage accumulation assessment before the year 1970. Limited data are available on which the model can be based. However, the damage accumulated up to 1970 is small compared to that after 1970 [66] and hence an approximate model suffices. As the differences between countries are deemed larger in the early days as compared to to-date, the model can be replaced by alternatives such as [40]. Load Model III is set-up as simple and conservative and it is based on interviews with experts. Because the traffic was dominated by cargo in this period, two categories are distinguished based on the type of cargo transport:

- Main tracks between main stations, generally characterized by a high density of cargo traffic with long trains, which are often composed by linking multiple shorter trains.
- Side tracks between towns or small industrial plants and main stations.

The maximum axle load has increased in time, see the dots in Fig. 12 for the axle loads in The Netherlands. To consider this in the load model, a distinction is made between cargo trains before and after 1945. For ease of use, a single train composition is used in these two periods (Appendix) but the axle loads of the wagons are different for the period before 1945 and the period between 1945 and 1970, following the dashed line in Fig. 12. A similar procedure can be adopted for other national trends in axle loads or, in lack of data, the trend of the UIC leaflet 779-1 [67] can be used as applied in [41]. The vehicle speed is taken as the maximum of the overview in [68].

A passenger train is added to both categories. A historical overview is made of passenger trains, see the background report [64]. The 'plan+loc' train, which is a train pulled by a locomotive, is selected for Load Model III because it represents most passenger traffic between 1900 and 1970 and because it causes the largest damage per unit load of all historic train types for all studied influence lines. The Appendix describes the five trains comprising Load Model III. Application of Load Model III requires a selection of the category and estimates of the number of cargo and passenger trains. Such data can be retrieved e.g. from historic timetables. Alternatively, the number of trains can be estimated as the estimated historic annual summed mass of cargo and passenger transport divided by the train masses of the model.

5. Reliability analyses

5.1. Measurement errors

The measurement systems have a guaranteed (calibrated) load measurement accuracy, with maximum errors of $\pm 10\%$ for axles, $\pm 5\%$ for wagons and $\pm 3\%$ for trains. The reduction of the error with increasing number of axles involved indicates that the error is a scatter on axle

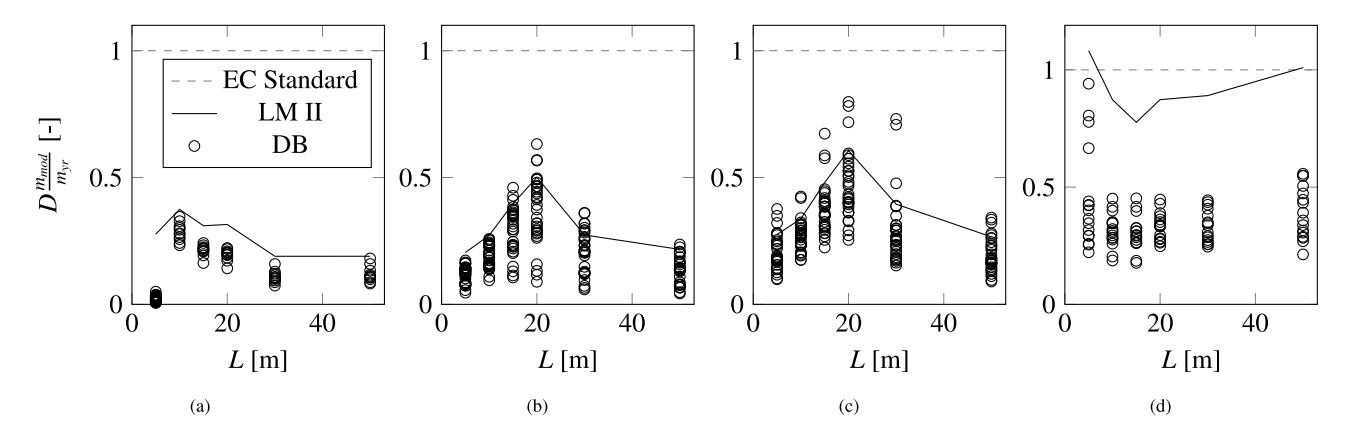


Fig. 10. Normalized fatigue damage of a welded connection in a single span beam using the EC standard traffic mix, Load Model II and the DB: (a) Category A+; (b) Category B+; (c) Category C+; (d) Category D+.

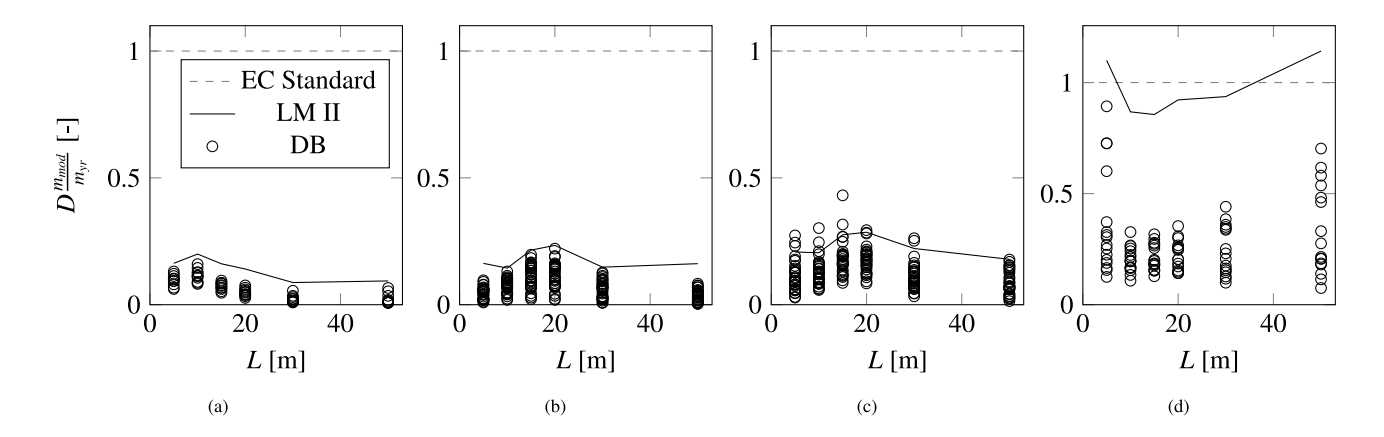


Fig. 11. Normalized fatigue damage of a riveted connection in a single span beam using the EC standard traffic mix, Load Model II and the DB: (a) Category A+; (b) Category B+; (c) Category C+; (d) Category D+.

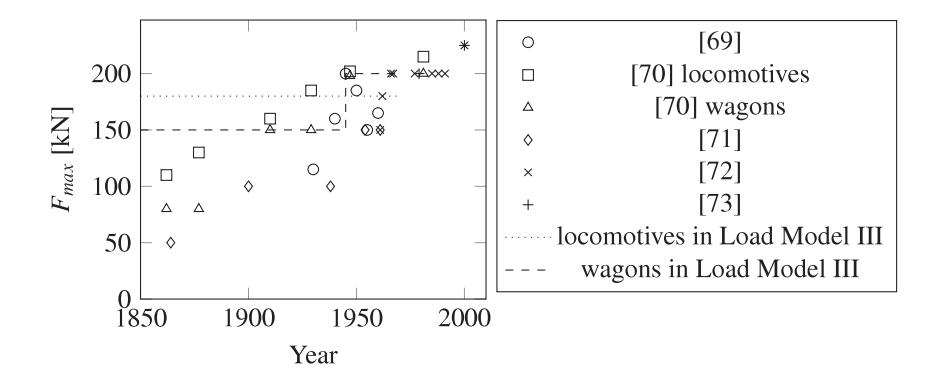


Fig. 12. Historic maximum axle load F_{max} in time for the Dutch railway network. (see [69–73]).

loads, not a bias. It is assumed that the error ε is normal distributed and that the 10% fraction reported for axles is exceeded with 2.5%:

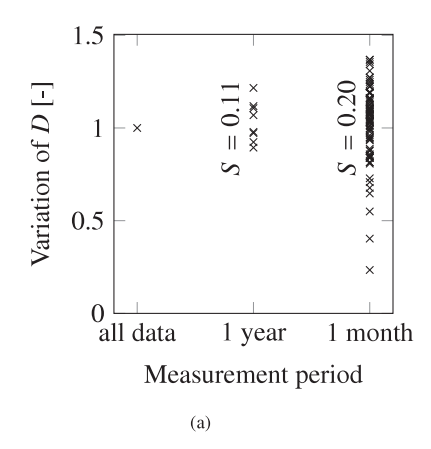
$$\varepsilon \in \mathcal{N}(0, 0.05) \tag{9}$$

where $\mathcal{N}(M,S)$ denotes the normal distribution with mean M and standard deviation S. The influence of the measurement error on the fatigue damage is assessed in a Monte Carlo (MC) analysis, in which

each actual axle load $F_{act,i}$ is randomly selected using:

$$F_{act,i} = F_{ax,i}(1+\varepsilon) \tag{10}$$

The fatigue damage D_{act} is determined in the same way as before, i.e. using Eqs. (3)–(4). The result is expressed through the ratio D_{act}/D_{DB} , where D_{DB} is the damage excluding the error, i.e. as in Section 3. The ratio is evaluated for a selection of influence lines and



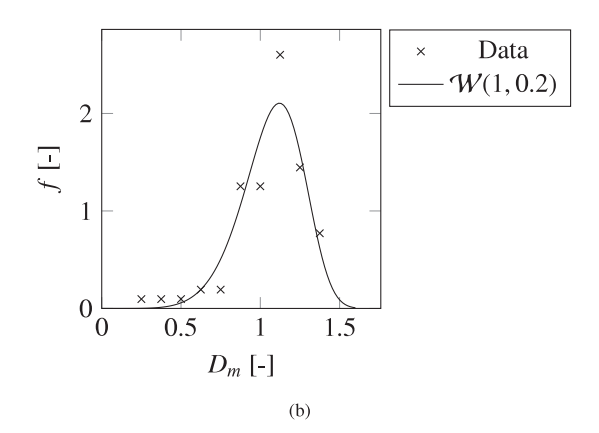


Fig. 13. Damage of location S512 evaluated per measurement period: (a) variation of damage; (b) damage distribution (probability density f) per month.

locations. The mean of the ratio is calculated as M=1.08 and 1.03 for spans of 5 m and 50 m, respectively. For both spans the standard deviation of the ratio is S=0.01.

5.2. Database size

The measurement period is quite long, but obviously shorter than the life of a bridge. The effect of the DB size is evaluated by determining the damage of the individual months, the individual years, and the entire measurement period of 89 months. Fig. 13(a) gives an example of the results for one of the heaviest loaded locations. As observed, the standard deviation of the damage per month is equal to 0.20. This is exemplary for all locations and it implies that a representative measurement period for fatigue of railway bridges is significantly larger than the few days that appeared sufficient for highway bridges [52]. Some variability will also be present in the damage of the entire measurement period. To estimate this variability, a MC analysis is carried out using the distribution of damage per month D_m , assuming independence between months:

$$D_{89} = \frac{1}{89} \sum_{a=1}^{89} D_m \tag{11}$$

$$D_m \in \mathcal{W}(1, 0.20) \tag{12}$$

where W(M,S) is the two-parameter Weibull distribution (Fig. 13(b)) with mean and standard deviation in normal space. The value of 89 stands for the number of months covering the measurement period. The results are expressed through the ratio D_{89}/D_{DB} , which results in V=0.02. This implies a negligible scatter.

5.3. Derivation of the partial safety factor

Structures should meet a certain legislative or standardized structural reliability. In practical assessments, this is achieved by multiplying all axle loads in the load model with a partial safety factor γ_F and dividing the resistance expressed through stress range in the characteristic S–N curve by γ_M . The European standard EN 1993-1-9 [74] recommends $\gamma_M=1.35$ for non-inspected details with large consequences of failure and a lower factor for inspected details. The factor γ_F is set irrespective of the inspection and failure consequences (i.e. this is considered through the resistance side). This section estimates the relationship between the structural reliability and γ_F for the newly developed load models. The estimation is largely equivalent to the derivation in [75] for road bridges, but it uses the relevant variables for the new railway load models. The estimate comprises of two steps. Step 1 considers the practical assessment using deterministic models.

A range of partial safety factors γ_F is applied and for each value, the corresponding elastic section modulus W is determined such, that the assessed damage $D_{des}=1$, using:

$$D_{des} = \sum_{j} \frac{n}{N_{des,j}} \tag{13}$$

where n is the number of days in 100 years (n = 36525) since the load models give the trains per day. The S–N curve format of the European pre-standard prEN 1993-1-9 [76] is adopted to determine the number of cycles to failure $N_{des,j}$:

$$N_{des,j} = \begin{cases} C_{1} (\Delta \sigma_{j} \gamma_{M} \gamma_{F})^{m_{1}} & \text{if } C_{1} (\Delta \sigma_{j} \gamma_{M} \gamma_{F})^{m_{1}} \leq N_{tr} \\ \infty & \text{if } C_{1}^{\frac{m_{2}}{m_{1}}} N_{tr}^{\frac{m_{1} - m_{2}}{m_{1}}} (\Delta \sigma_{j} \gamma_{M} \gamma_{F})^{m_{2}} \geq 10^{8} \\ C_{1}^{\frac{m_{2}}{m_{1}}} N_{tr}^{\frac{m_{1} - m_{2}}{m_{1}}} (\Delta \sigma_{j} \gamma_{M} \gamma_{F})^{m_{2}} & \text{otherwise} \end{cases}$$
(14)

in which C_1 and N_{tr} are the 95% survival fraction values. A welded cover plate is used as an exemplary fatigue sensitive detail, for which $N_{tr}=10^7, m_1=-3, m_2=-5,$ and $C_1=11.4$ for $\Delta\sigma$ expressed in N/mm². Using the same W as in Step 1, a MC analysis is employed in Step 2 to estimate the corresponding structural reliability, using a probabilistic S–N curve according to [77,78] and the relevant uncertainties related to the load side:

$$\log_{10}(N_{p,j}) = \begin{cases} C_p + m_p \log_{10}(\Delta \sigma_j C_{mu} \frac{C_{daf}}{\phi}) - \eta \log_{10} \left(1 - \frac{\Delta \sigma_{th}}{\Delta \sigma_j C_{mu} \frac{C_{daf}}{\phi}} \right) \\ \text{if } \Delta \sigma_j C_{mu} \frac{C_{daf}}{\phi} > \Delta \sigma_{th} \\ \infty \\ \text{otherwise} \end{cases}$$

 $\Delta \sigma_{th} = \Delta \sigma_0 \left(1 - \frac{D_p}{D_{cr}} \right)^{\zeta} \tag{16}$

$$D_{p} = \sum_{j} \frac{n}{N_{p,j}} \frac{D_{DB}}{D_{mod}} \frac{D_{act}}{D_{DB}} \left(1 + \sum_{q=1}^{13} \left[\frac{D_{89}}{D_{DB}} - 1 \right] \right)$$
 (17)

where subscript p is added to distinguish the probabilistic variables from the design values, D_{cr} is the critical damage causing failure, $\Delta\sigma_0$ is the fatigue limit, $\Delta\sigma_{th}$ is the fatigue threshold which reduces with damage, and η and ζ are model variables representing the transition from finite life to near-infinite life and the damage evolution, respectively. The stress ranges $\Delta\sigma_j$ are determined with either Load Model I or II and D_{mod} is the corresponding value of D_{LM1} or D_{LMII} (Section 4). Load

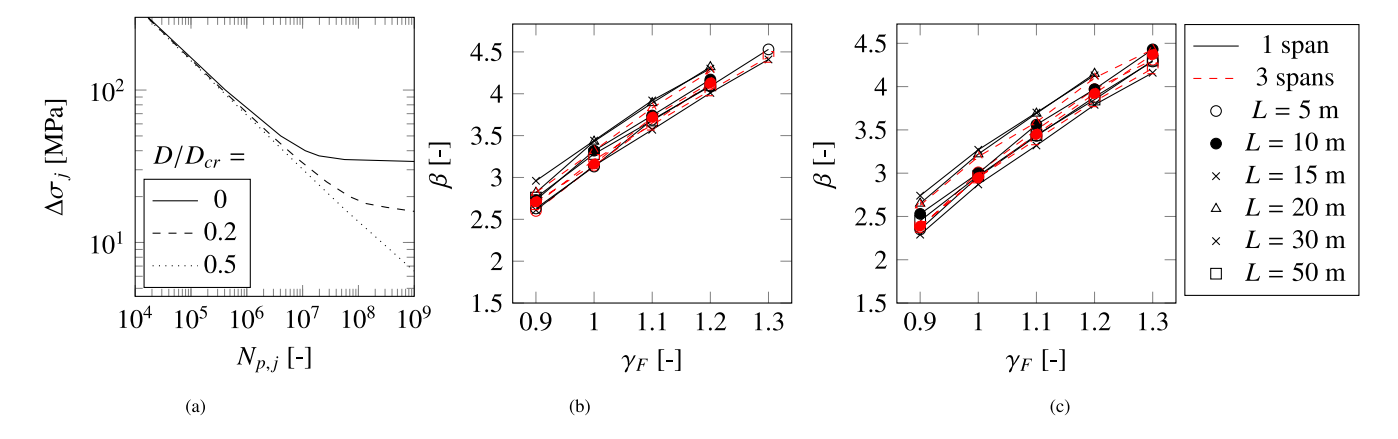


Fig. 14. Reliability analysis for a standard deviation of 0.05 for C_{daf}/ϕ : (a) Probabilistic S–N curve with mean values; (b) Reliability index (full life) for Load Model II.

Model III cannot be assessed because of a lack of measurement data, but it is developed as a conservative load model and its contribution to the total damage is small. The value of 13 in Eq. (17) refers to the integer of the ratio between the life span and the measurement period. Note that simulation is done for a 100 years life, but a different life will only marginally affect the results because n is used in both Eqs. (13) and (17) and the last term of Eq. (17) is close to unity. Variable C_{mu} is an engineering model uncertainty representing the accuracy of the estimated influence line and C_{daf} is the uncertainty in the dynamic amplification. Eqs. (15)–(17) need to be solved iteratively because Eq. (16) implies that $\Delta\sigma_{th}$ reduces as D_p evolves, see Fig. 14(a).

Based on measurements and models in [29,79,80], the model uncertainty distribution used in [30] is $\mathcal{N}(0.8,0.14)$. In addition to the influence line estimation, their model uncertainty includes the deviation between the load model and the actual load, which is considered separately through the ratio $\frac{D_{DB}}{D_{mod}}$ in the current study. Imam et al. [30] give causes of higher mean computed load effects as compared to actual load effects. However, this depends on the level of detail considered in the computation: Accurate or even non-conservative load effects were computed in [11,81], respectively. A large standard deviation of the model uncertainty is obtained in [82]. The model uncertainty factor $C_{mu} \in \mathcal{L}(1,0.1)$ proposed in the JCSS probabilistic model code [83] is adopted in the current study.

Test campaigns are available from which ${\cal C}_{daf}$ can be estimated. The most extensive data source that the authors have found is a study from 1960 [84], where the load effect of 1800 passing diesel and electric locomotives on various steel bridges in the United States was compared to the static load effect of the same locomotives. Bridges with ballast floors had lower dynamic amplifications compared to bridges with open deck girders. The data of the latter type are fit to normal distributions in [80] and to lognormal distributions in [85]. The dynamic amplification factor is normalized here by dividing the lognormal distribution by the dynamic amplification factor of EN 1991-2 [20], i.e. Eqs. (1)-(2). This gives $C_{daf}/\phi = \mathcal{L}(1.03, 0.09)$, which would imply that ϕ in the standard is unconservative. However, C_{daf} according to these measurements is expected to be too high for current practice and for fatigue calculations, because trains and rails are currently designed for lower impacts as in the years 1960 - which is confirmed by comparing the data in [84] to more recent, comparable but less extensive, campaigns on ballasted floor bridges in [86] and open deck bridges in [11,43,79] - because the impact reduces with an increase in (static) load as demonstrated in [87] for road bridges, and because the impact at a certain structural detail is expected to show scatter, whereas the formulation adopted with Eqs. (15)-(17) implies that the dynamic impact factor is equal for all crossings. The distribution of the dynamic amplification factor ratio used here is $C_{daf}/\phi = \mathcal{L}(1.0, 0.05)$ but the simulations are repeated

Table 6
Distributions of the random variables (units: N, mm).

Symbol	Value or distribution ^a	Source
m_p^{b} C_p^{b} $\Delta\sigma_0^{\mathrm{b}}$	-2.78	[77]
$C_p^{\mathbf{b}}$	$\mathcal{N}(11.09, 0.13)$	[77]
$\Delta \sigma_0^{\ \mathbf{b}}$	$\mathcal{L}(34.7, 4.5)$	[77]
$\eta^{ m b}$	0.47	[77]
$\zeta^{ m b}$	3.27	[78]
D_{cr}^{b}	$\mathcal{L}(1.46, 0.25)$	[78]
C_{mu}	$\mathcal{L}(1.0, 0.10)$	[83]
C_{daf}/ϕ	$\mathcal{L}(1.0, 0.09)$ or $\mathcal{L}(1.0, 0.05)$	Section 5.3
$D_{DB}/D_{LMI}^{^{^{}}}$	W(0.52, 0.28)	Section 4.1
D_{DB}/D_{LMII}^{c}	W(0.68, 0.31)	Section 4.2
D_{act}/D_{DB}	$\mathcal{N}(1.08 - L/10^6, 0.01)$	Section 5.1
D_{89}/D_{DB}	$\mathcal{N}(1, 0.02)$	Section 5.2

 ${}^a\mathcal{N}(M,S)=$ normal distribution, $\mathcal{L}(M,S)=$ lognormal distribution, $\mathcal{W}(M,S)=$ two parameter Weibull distribution. In all cases M and S in normal space.

^bDistribution parameters are point estimates for a cover plate detail. Standard errors and correlations are also taken into account, with values in [77,78].

 c The Weibull distribution gave the best fit of three considered candidate distributions $\mathcal{N},\,\mathcal{L}$ and $\mathcal{W}.$

with an increased standard deviation of S=0.09 to study its influence. Table 6 gives the distributions of the random variables.

The limit state function *g* is:

$$g = D_{cr} - D_{p} \tag{18}$$

The failure probability P_f is estimated from a number of n_{mc} MC runs:

$$P_f = \frac{1}{n_{mc}} \sum_{p=1}^{n_{mc}} H(-g_p)$$
 (19)

where H is the Heaviside step function and g_p is the limit state evaluation for MC run p. To obtain a specific accuracy in the reliability estimate, the MC simulation is continued until the summation term in Eq. (19) reaches a value of 100, thereby defining n_{mc} . The corresponding reliability index for the full life period β is determined with:

$$\beta = -\Phi^{-1}(P_f) \tag{20}$$

where Φ^{-1} is the inverse of the cumulative standard normal distribution.

Target reliability indices for fatigue provided in standards depend on the consequences of failure, inspections, and possibilities of repair. The standard EN 1990 [88] recommends $1.5 \le \beta \le 4.3$ for new structures, where β refers to the full design life. ISO 2394 [89] gives annual values that are largely consistent with those in EN 1990 [88], see [75]. For fatigue of existing structures, ISO 13822 [90] recommends

 $2.3 \leq \beta \leq 3.1$, referring to the remaining working life. National standards can give deviating values. Studies carried out around 1990 by Moses et al. used $\beta=2$ [91] for the remaining working life. The relation between γ_F and β is evaluated for the full range of the mentioned β values, with results in Fig. 14(b) and (c) for a safe life assessment and a standard deviation of C_{daf}/ϕ equal to S=0.05. The figure indicates that the relation is only marginally depending on the influence line. A partial safety factor of $\gamma_F=1.0$ gives an estimated reliability index of $\beta\approx 3.2$ or 3.0 for Load Model I or II, respectively. The reliability index reduces with 0.15 if the standard deviation of C_{daf}/ϕ is increased to S=0.09. Note that these results are valid if the dynamic amplification factor of Eqs. (1)–(2) is applied and if the S–N curve and the partial safety factor for the resistance of EN 1993-1-9 [74] are applied in the assessment.

A similar derivation of the partial safety factor as given here cannot be performed for riveted connections because this requires constant amplitude (run-out) test data in the very high cycle domain ($N > 10^7$) and variable amplitude test data in the high cycle and the very high cycle domains, including failures and run-outs. Such data are lacking for riveted connections. However, given that the load models show a similar level of conservatism as for welded connections (Section 4) similar results as those in Fig. 14 are expected for riveted connections.

6. Conclusions

The work presented in this paper describes three fatigue load models based on axle load measurements between 2012 and 2019 at 87 locations in the rail network of The Netherlands (high-speed tracks excluded). Fatigue damage calculated using these measurements is compared to fatigue damage calculated using the load model from the European standard EN 1991-2 Annex D [20]. The three fatigue load models are developed for the purpose of fatigue assessment of existing structures. The models are aimed for desk study, in case bridge specific (strain) measurements are not available. Different from other fatigue load models proposed in the literature, the load models proposed here differentiate in the rail traffic (daily train composition) based on the use of the track. The models are therefore track-specific, causing them to more closely resemble the real fatigue load effects compared to generic models. The following conclusions apply:

- The damage computed using measured axle loads differs significantly between tracks. For assessing existing structures, it is therefore beneficial to differentiate in the load model based on the use of the track.
- The equivalent axle load, the fraction of cargo transport, the dominant type of passenger train (especially in case of double deck trains with large boogie distances) and the number of axles (or annual transported mass) are the important usage characteristics. These have been accounted for in deriving the three alternative fatigue load models.
- Because of the larger variability in axle loads between subsequent full and empty wagons in a cargo train, their axles generally give a larger contribution to the fatigue damage compared to a passenger train axle of the same load.

- Compared to the axle load measurements, the EN 1991-2 Annex D
 fatigue load model is safe yet very conservative for most locations,
 but it is unconservative for a few locations. Not all trains in the
 load model are representative for today's rail traffic.
- The new models give a better approximation of the fatigue damage as compared to the EN 1991-2 Annex D fatigue load model. The coefficients of variation of the ratio in damage between the measurements per location and the load model of EN 1991-2 Annex D are 1.3 and 1.9 for a welded and a riveted connection, respectively. The coefficient of variation ranges between 0.45 and 0.67 for the new load models. The new load models give a reliability index slightly larger than 3 in case of a partial safety factor on the load side of 1 and a resistance as defined in the standard EN 1993-1-9 [74].
- The annual summed mass alone is an insufficiently accurate indicator of the fatigue damage. The axle loads and axle distances appear also important and they depend on the use of the track. A clear correlation exists between the equivalent axle load (Eq. (5)) and the number of axles on the one hand, and the fatigue damage on the other hand.
- Significant uncertainty exists in the dynamic amplification factor
 and in the accuracy of the engineering model of the influence line.
 Measurement campaigns should be carried out to evaluate these
 uncertainties for current track, trains and models. Additionally,
 variable amplitude fatigue test data on riveted connections are
 lacking. The probabilistic assessment of existing structures may
 benefit from studies on these aspects.

Declaration of competing interest

The authors declare that they have no known competing financial interests or personal relationships that could have appeared to influence the work reported in this paper.

Data availability

The authors do not have permission to share data.

Acknowledgments

This research was sponsored by the Dutch Railway asset owner ProRail. The authors would like to thank Ron van der Zwan, Arend Kremer, Juliette van Driel and Maurice van Olderen for explaining the measurement system and providing information on train compositions.

Appendix. Train types

This appendix lists the characteristics of the 12 trains from the new Load Models I and II, followed by the trains from the historical trains Load Model III (see Figs. A.15–A.29).

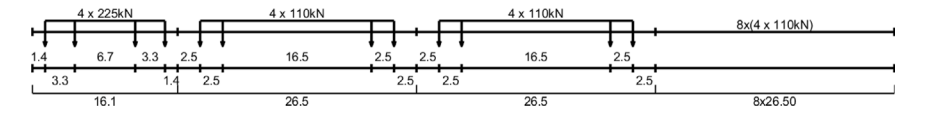


Fig. A.15. Type 2 of EN 1991-2 Annex D; v = 160 km/h (distances in [m]).

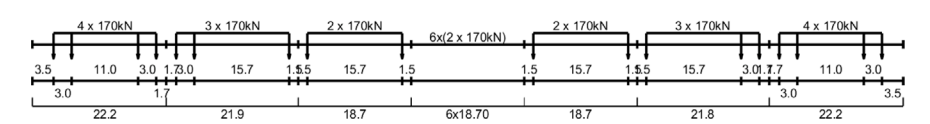


Fig. A.16. Type 4 of EN 1991-2 Annex D; v = 250 km/h (distances in [m]).

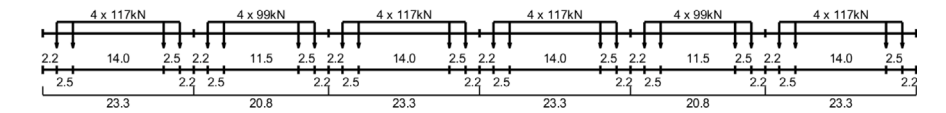


Fig. A.17. Type 9 of EN 1991-2 Annex D, with all axle loads multiplied by a factor 0.9; v = 120 km/h (distances in [m]).

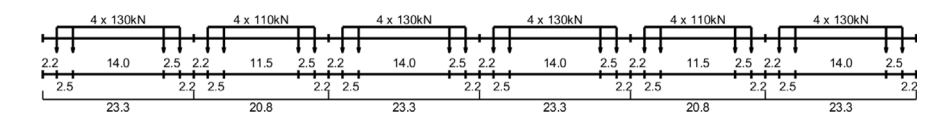


Fig. A.18. Type 9 of EN 1991-2 Annex D; v = 120 km/h (distances in [m]).



Fig. A.19. Passenger train based on GTW trains; v = 140 km/h (distances in [m]).

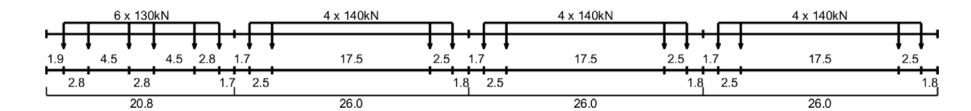


Fig. A.20. Passenger train based on DDAR/DDZ trains; v = 140 km/h (distances in [m]).

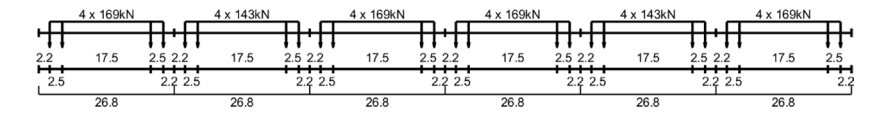


Fig. A.21. Passenger train based on VIRM trains; v = 120 km/h (distances in [m]).

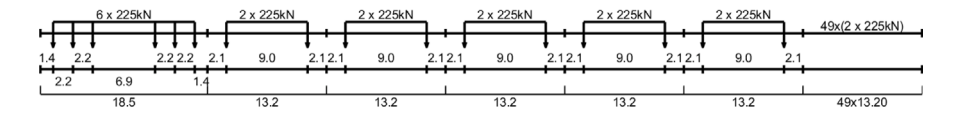


Fig. A.22. Cargo train with full 2-axle wagons; v = 100 km/h (distances in [m]).

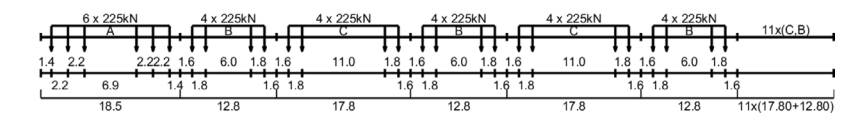


Fig. A.23. Cargo train with full 4-axle wagons; v = 100 km/h (distances in [m]).

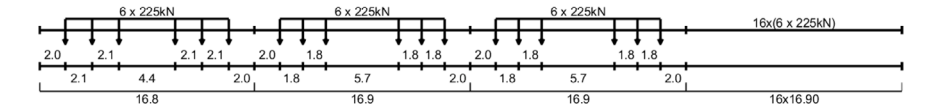


Fig. A.24. Cargo train with full 6-axle wagons; v = 80 km/h (distances in [m]).

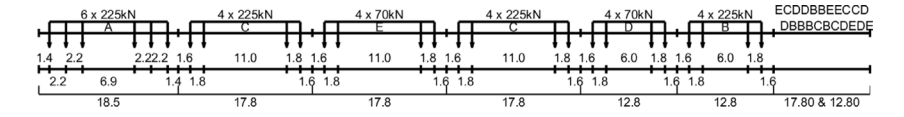


Fig. A.25. Cargo train with full and empty 4-axle wagons; v = 100 km/h (distances in [m]).

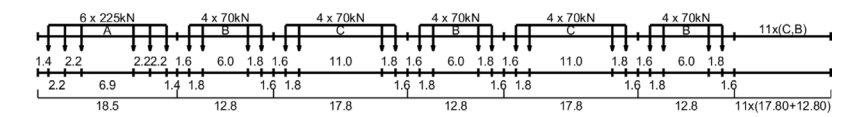


Fig. A.26. Cargo train with empty 4-axle wagons; v = 100 km/h (distances in [m]).

Fig. A.27. Historical main track cargo train (LM III); v = 60 km/h (distances in [m]), where $F_{ax} = 150$ kN for the period 1900–1945 and $F_{ax} = 200$ kN for the period 1945–1970.

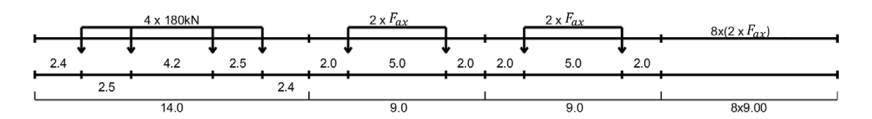


Fig. A.28. Historical side track cargo train (LM III); v = 60 km/h (distances in [m]), where $F_{ax} = 150$ kN for the period 1900–1945 and $F_{ax} = 200$ kN for the period 1945–1970.

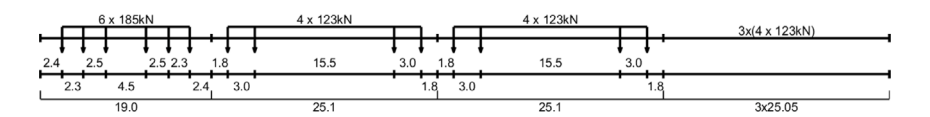


Fig. A.29. Historical passenger train (LM III); v = 125 km/h (distances in [m]).

References

- [1] Bień J, Jakubowski K, Kamiński T, Kmita J, Kmita P, Cruz P, et al. Railway bridge defects and degradation mechanisms. In: Sustainable bridges: Assessment for future traffic demands and longer lives. 2007, p. 105–16.
- [2] Piechota M, Rogojsz G. Analysis of the technical condition of a railway bridge at risk of failure. In: MATEC web of conferences. vol. 284, EDP Sciences; 2019, p. 01005
- [3] Haghani R, Al-Emrani M, Heshmati M. Fatigue-prone details in steel bridges. Buildings 2012;2:456–76.
- [4] Li H, Soliman M, Frangopol DM, Xia H. Fatigue damage in railway steel bridges: Approach based on a dynamic train-bridge coupled model. J Bridge Eng 2017;22(11):06017006.
- [5] Pimentel M, Brühwiler E, Figueiras J. Fatigue life of short-span reinforced concrete railway bridges. Struct Concrete 2008;9(4):215–22.
- [6] Raoult I, Delattre B. Equivalent fatigue load approach for fatigue design of uncertain structures. Int J Fatigue 2020;135:105516.
- [7] Cremona C, Eichler B, Johansson B, Larsson T. Improved assessment methods for static and fatigue resistance of old metallic railway bridges. J Bridge Eng 2013;18(11):1164–73.
- [8] Ye X, Su Y, Han J. A state-of-the-art review on fatigue life assessment of steel bridges. Math Probl Eng 2014;2014.
- [9] Li Z, Chan T, Zheng R. Statistical analysis of online strain response and its application in fatigue assessment of a long-span steel bridge. Eng Struct 2003;25(14):1731–41.
- [10] Ni Y, Ye X, Ko J. Monitoring-based fatigue reliability assessment of steel bridges: analytical model and application. J Struct Eng 2010;136(12):1563–73.
- [11] Leander J, Andersson A, Karoumi R. Monitoring and enhanced fatigue evaluation of a steel railway bridge. Eng Struct 2010;32(3):854–63.
- [12] Moyo P, Tait R. Structural performance assessment and fatigue analysis of a railway bridge. Struct Infrastruct Eng 2010;6(5):647–60.
- [13] Ye X, Ni YQ, Wong K, Ko J. Statistical analysis of stress spectra for fatigue life assessment of steel bridges with structural health monitoring data. Eng Struct 2012;45:166–76.
- [14] Pipinato A, Pellegrino C, Modena C. Residual life of historic riveted steel bridges: an analytical approach. Proc Inst Civil Eng - Bridge Eng 2014;167(1):17–32.
- [15] Marques F, Correia JA, de Jesus AM, Cunha A, Caetano E, Fernandes AA. Fatigue analysis of a railway bridge based on fracture mechanics and local modelling of riveted connections. Eng Fail Anal 2018;94:121–44.
- [16] Chmielewski R, Muzolf P. Analysis of degradation process of a railway steel bridge in the final period of its operation. Struct Infrastruct Eng 2021;1–17.
- [17] Bertolesi E, Buitrago M, Adam JM, Calderon PA. Fatigue assessment of steel riveted railway bridges: Full-scale tests and analytical approach. J Construct Steel Res 2021;182:106664.
- [18] Kühn B, Lukic M, Nussbaumer A, Günther H, Helmerich R, Herion S, et al. Assessment of existing steel structures: recommendations for estimation of remaining fatigue life. Joint Research Center; 2008.
- [19] Leander J, Honfi D, Ivanov OL, Björnsson Í. A decision support framework for fatigue assessment of steel bridges. Eng Fail Anal 2018;91:306–14.
- [20] EN1991-2:2003. Eurocode 1: Actions on structures Part 2: Traffic loads on bridges. CEN: 2003.
- [21] ERRI:1996. UIC Leaflet 702 Loading diagram to be taken into consideration for the calculation of rail carrying structures on lines used by international services. International Union of Railways; 2003.

- [22] Lippi FV, Orlando M, Salvatore W. Assessment of the dynamic and fatigue behaviour of the Panaro railway steel bridge. Struct Infrastruct Eng 2013;9(8):834–48.
- [23] Horas CS, De Jesus AM, Calçada R. Efficient progressive global-local fatigue assessment methodology for existing metallic railway bridges. J Construct Steel Res 2022;196:107431.
- [24] Kossakowski PG. Fatigue strength of an over one hundred year old railway bridge. Balt J Road Bridge Eng 2013;8(3):166–73.
- [25] NN. Istruzione N. 44/F Verifiche a fatica dei ponti ferroviari metallici (Instruction N. 44/F: Fatigue verification of metal railway bridges). Tech. rep., Italian Railway Authority, Milan, Italy; 1992.
- [26] Pipinato A, Pellegrino C, Modena C. Assessment procedure and rehabilitation criteria for the riveted railway Adige Bridge. Struct Infrastruct Eng 2012;8(8):747-64.
- [27] BS 5400:2006. British Standard 5400 Steel, concrete and composite bridges. Specification for loads. British Standards Institution; 2006.
- [28] Imam B, Righiniotis T, Chryssanthopoulos MK. Numerical modelling of riveted railway bridge connections for fatigue evaluation. Eng Struct 2007;29:3071–81.
- [29] Adamson D. Fatigue tests of riveted bridge girders. University of Alberta; 1995.
- [30] Imam BM, Righiniotis TD, Chryssanthopoulos MK. Probabilistic fatigue evaluation of riveted railway bridges. J Bridge Eng 2008;13:237–44.
- [31] Marques F, Cunha Á, Fernandes AA, Caetano E, Magalhães F. Evaluation of dynamic effects and fatigue assessment of a metallic railway bridge. Struct Infrastruct Eng 2010;6(5):635–46.
- [32] Rakoczy AM, Nowak AS, Dick S. Fatigue reliability model for steel railway bridges. Struct Infrastruct Eng 2016;12:1602–13.
- [33] Basso P, Casciati S, Faravelli L. Fatigue reliability assessment of a historic railway bridge designed by Gustave Eiffel. Struct Infrastruct Eng 2015;11:1:27–37.
- [34] Marques F, Moutinho C, Hu W-H, Cunha Á, Caetano E. Weigh-in-motion implementation in an old metallic railway bridge. Eng Struct 2016;123:15–29.
- [35] Zakharenko M, Frøseth GT, Rönnquist A. Train classification using a weigh-inmotion system and associated algorithms to determine fatigue loads. Sensors 2022;22(5):1772.
- [36] Hajializadeh D, Žnidarič A, Kalin J, OBrien EJ. Development and testing of a railway bridge weigh-in-motion system. Appl Sci 2020;10(14):4708.
- [37] James G. Analysis of traffic load effects on railway bridges [Ph.D. thesis], KTH Royal Institute of Technology; 2003.
- [38] James G. Analysis of traffic load effects on railway bridges using weigh-in-motion data. In: Fourth international conference on weigh-in-motion (ICWIM4), February 20–22, Taipei, Taiwan. 2005.
- [39] Žnidarič A, Kalin J, Kreslin M, Favai P, Kolakowski P. Railway bridge Weigh-in-Motion system. Transp Res Procedia 2016;14:4010–9.
- [40] Imam B, Righiniotis T, Chryssanthopoulos M. Probabilistic fatigue load spectra for riveted railway bridges. In: Proceedings of the 10th international conference on applications of statistics and probability in civil engineering. 2007, p. 73–4.
- [41] Pipinato A, Pellegrino C, Modena C. Fatigue damage estimation in existing railway steel bridges by detailed loading history analysis. Int Schol Res Not 2012:2012.
- [42] Imam B, Salter PA. Historical load effects on fatigue of metallic railway bridges. Bridge Eng 2017;171:49–62.
- [43] Tobias D, Foutch D, Choros J. Loading spectra for railway bridges under current operating conditions. J Bridge Eng 1996;1(4):127–34.
- [44] Tobias D, Foutch D. Reliability-based method for fatigue evaluation of railway bridges. J Bridge Eng 1997;2(2):53–60.

- [45] Rakoczy AM, Liu S, Otter D, Dick S. Current loading spectra for evaluation of railway bridges. Technol Digest 2018;2018.
- [46] Frøseth GT, Rönnquist A. Load model of historic traffic for fatigue life estimation of Norwegian railway bridges. Eng Struct 2019;200:109626.
- [47] Imam B, Righiniotis T, Chryssanthopoulos M. Remaining fatigue life estimates for riveted railway bridges. In: Bridge management five: Proceedings of the 5th international conference on bridge management. 2005, p. 417–25.
- [48] Imam B. Fatigue analysis of Rivited Railway Bridges [Ph.D. thesis], University of Surrey; 2006.
- [49] Skagestad AB, Sørbel I. Evaluation of the consistent load model for Norwegian railway bridges subjected to fatigue considering track curvature and non-standard influence lines [Ph.D. thesis], Norwegian University of Science and Technology; 2021.
- [50] van Driel J. Quo Vadis and Hotbox on the measurements of train weights, axle and wheel temperatures [Quo Vadis en Hotbox - voor het meten het gewicht van rijdende treinen en de temperatuur van assen en wielen]. ProRail; 2018.
- [51] List of trains in the Netherlands. Wikipedia; 2022, URL https://en.wikipedia.org/ wiki/List of trains in the Netherlands.
- [52] Maljaars J. Evaluation of traffic load models for fatigue verification of European road bridges. Eng Struct 2020;225:111326.
- [53] Palmgren A. Die lebensdauer von Kugellagern. Zeitschrift 1924;68:339-41.
- [54] Miner M. Cumulative damage in fatigue. Trans ASME J Appl Mech 1945;12:A159–64.
- [55] Silva A, Correia JA, Xin H, Lesiuk G, De Jesus AM, Fernandes AA, et al. Fatigue strength assessment of riveted details in railway metallic bridges. Eng Fail Anal 2021;121:105120.
- [56] Pipinato A, Molinari M, Pellegrino C, Bursi O, Modena C. Fatigue tests on riveted steel elements taken from a railway bridge. Struct Infrastruct Eng 2011:7(12):907-20.
- [57] Taras A, Greiner R. Development and application of a fatigue class catalogue for riveted bridge components. Struct Eng Int 2010;20(1):91–103.
- [58] Jia D, Zhang Q, Xiong L, Li J, Bu Y, Bao Y. A unified evaluation method for fatigue resistance of riveted joints based on structural stress approach. Int J Fatigue 2022:160:106871.
- [59] Maljaars J, Euler M. Fatigue SN curves of bolts and bolted connections for application in civil engineering structures. Int J Fatigue 2021;151:106355.
- [60] Haibach E. The allowable stresses under variable amplitude loading of welded joints. In: Conference fatigue of welded structures, vol. 2, 1971, p. 328–39.
- [61] Crocetti R, Al-Emrani M, Åkesson B, Edlund B. Constant amplitude fatigue limit for riveted girders. Acta Polytecnica-Eurosteel 1999;39(5).
- [62] van der Zwan R. SAP-Data ProRail information on railway bridges in The Netherlands. ProRail; 2021.
- [63] Helmerich R, Kühn B, Nussbaumer A. Assessment of existing steel structures: A guideline for estimation of the remaining fatigue life. Struct Infrastruct Eng 2007;3(3):245-55.
- [64] Verdenius S, Hengeveld S, Maljaars J, Braendstrup C. Customized fatigue load models for railway bridges, TNO 2022 R10610 (available on request). TNO; 2022
- [65] Bakker D. Up to date track loading based on Quo Vadis measurement Data [Actuele spoorbelasting op basis Van Quo Vadis Data]. Ricardo Rail; 2016.
- [66] Artukka A. Estimating the remaining service life of concrete railway bridge. Finnish Transport Agency; 2014, [in finnish].
- [67] NN. UIC Leaflets 779-1 R: recommendations for the evaluation of the load carrying capacity of existing steel bridges. Tech. rep., International Union of Railways, Utrecht, The Netherlands; 1998.

- [68] Steur D, Lommers N, Bakker D. Analysis of historic rail load 1938–2015. Ricardo Rail; 2017, [in Dutch].
- [69] Materiaalgegevens Locomotieven historie NS en Stoom DB, volgnummer 612. ProRail; 1970.
- [70] van der Zwan R. Axle load document provided by ProRail. ProRail; 1970.
- [71] Van de Weerd G. Train fanatics reporting on passenger and cargo trains used by NS over time. G. van de Weerd; 2022, URL https://www.seinarm.nl [in Dutch].
- [72] Ankersmit R. Interview with NVSB (Nederlandse Vereniging Van Belangstellenden in het Spoor- en tramwegwezen). TNO; 2022.
- [73] Lunteren Bv, Bleumink G. Interview with former ProRail-employees. TNO; 2022.
- [74] EN1993-1-9:2006. Eurocode 3: Design of steel structures Part 1-9: Fatigue. CEN; 2006.
- [75] Maljaars J, Leonetti D, Hashemi B, Snijder H. Systematic derivation of safety factors for the fatigue design of steel bridges. Struct Saf 2022;97.
- [76] prEN1993-1-9:2022. Pre-standard Eurocode 3 Design of steel structures Part 1-9: Fatigue. Final document 2021-08-05. CEN; 2021.
- [77] Leonetti D, Maljaars J, Snijder HH. Fitting fatigue test data with a novel S-N curve using frequentist and Bayesian inference. Int J Fatigue 2017;105:128–43.
- [78] Leonetti D, Maljaars J, Snijder HH. Probabilistic fatigue resistance model for steel welded details under variable amplitude loading-inference and uncertainty estimation. Int J Fatigue 2020;135:105515.
- [79] Sweeney RAP, Oommen G, Le H. Impact of site measurements on the evaluation of steel railway bridges. In: IABSE workshop. 1997, p. 139–48.
- [80] Byers WG. Impact from railway loading on steel girder spans. J Struct Div 1970;96(6):1093–103.
- [81] Marques F, Moutinho C, Magalhães F, Caetano E, Cunha Á. Analysis of dynamic and fatigue effects in an old metallic riveted bridge. J Construct Steel Res 2014;99:85–101.
- [82] Imam B, Kaliyaperumal G. Fatigue assessment of a railway bridge detail using dynamic analysis and probabilistic fracture mechanics. In: Bridge maintenance, safety, management, resilience and sustainability-proceedings of the sixth international conference on bridge maintenance, safety and management. 2012, p. 3206–13.
- [83] JCSS. JCSS probabilistic model code. Joint Committee of Structural Safety (JCSS); 2013, URL https://www.jcss-lc.org/jcss-probabilistic-model-code/.
- [84] Musser DW. Summary of tests on steel girder spans. In: Proceedings of the fiftyninth annual convention of the American Railway Engineering Association. vol. 61, 1960, p. 51–78.
- [85] Tobias DH. A method for the fatigue evaluation of riveted steel girder railway bridges [Doctoral thesis], University of Illinois at Urbana-Champaign; 1994.
- [86] Mensinger M, Fard R, Hacker A, Näßl A. Validation of the dynamic amplification factor in case of historic railway steel bridges with short and medium spans. Procedia Eng 2016;156:233–40.
- [87] Kalin J, Žinidarič A, Anžlin A, Kreslin M. Measurements of bridge dynamic amplification factor using bridge weigh-in-motion data. Struct Infrastruct Eng 2021:1-13.
- [88] EN 1990:2005. Eurocode Basis of structural design. CEN; 2005.
- [89] ISO 2394:2015. General principles on reliability for structures. ISO; 2015.
- [90] ISO 13822:2010. Bases for design of structures Assessment of existing structures. ISO; 2010.
- [91] Raju S, Moses F, Schilling C. Reliability calibration of fatigue evaluation and design procedures. J Struct Eng New York 1990;116(5):1356–69.